symmetry

MDPI

Article

Theoretical Survey of Time-Dependent Micropolar Nanofluid Flow over a Linear Curved Stretching Surface

Nadeem Abbas [1] and Wasfi Shatanawi [1,2,3,*]

[1] Department of Mathematics and Sciences, College of Humanities and Sciences, Prince Sultan University, Riyadh 11586, Saudi Arabia
[2] Department of Medical Research, China Medical University Hospital, China Medical University, Taichung 40402, Taiwan
[3] Department of Mathematics, Faculty of Science, The Hashemite University, P.O. Box 330127, Zarqa 13133, Jordan
* Correspondence: wshatanawi@psu.edu.sa

Abstract: The heat and mass transfer of the unsteady flow of a micropolar fluid over a curved stretching surface was considered in this study. The Brownian motion and thermophoresis effects were explored in this analysis. The effects of suction/injection cases on the curved surface were discussed. Under flow assumptions, a mathematical model was designed employing boundary layer approximations using partial differential equations. A suitable transformation was developed using the lie symmetry method. Partial differential equations were transformed into ordinary differential equations by suitable transformations. The dimensionless system was elucidated through a numerical technique, namely bvp4c. The involved physical parameters' influences are described in the form of graphs as well as numerical results in the form of tables. Our current work is helpful in the engineering and industrial fields. The unsteadiness parameter increases which Nusselt number at increased but concentrations declined. The thermophoresis parameter increases when increasing the Nusselt number because the small number of nanoparticles enhances the heat transfer rate. The temperature profile declined due to increasing values of unsteadiness parameter for both cases of suction and injection cases.

Keywords: micropolar fluid; buongiorno model; unsteady flow; curved surface; suction/injection case

Citation: Abbas, N.; Shatanawi, W. Theoretical Survey of Time-Dependent Micropolar Nanofluid Flow over a Linear Curved Stretching Surface. *Symmetry* **2022**, *14*, 1629. https://doi.org/10.3390/sym14081629

Academic Editors: Yifei Guan and Jian Wu

Received: 19 June 2022
Accepted: 26 July 2022
Published: 8 August 2022

1. Introduction

The heat and mass transfer of a nanofluid over a stretched curved surface has been studied. The combination of a base fluid with nanoparticles is known as a nanofluid. Mostly, nanoparticles in a nanofluid are a mixture of oxides, carbides, metals, and carbon nanotube with a base fluid. The heat transfer increases with the thermal conductivity of a nanofluid. The thermal conductivity of the nanofluid plays a vital role in the heat transfer phenomenon. The term nanofluid was first used by Choi and Eastman [1] in 1995. The size of nanoparticles is 1–100 nm and they are dispersed in a base fluid. Masuda et al. [2] observed the variations in the viscosity and thermal conductivity of liquid by the inclusion between base fluid and nanoparticles. Yu and Mittra [3] presented a simple (FDTD) technique which can be used to study curved dielectric surfaces. Nadeem and Lee [4] analytically considered a nanofluid over an exponentially stretching surface. They explored the results of Brownian motion and thermophoresis on a non-linear stretching surface. The based peristaltic hyperbolic tangent fluid flow at the curved channel examined was studied by Nadeem and Maraj [5]. Malvandi et al. [6] elucidated the characteristics of a nanofluid with heat generation over a porous stretching sheet. The effects of heat generation and chemical reaction of a second-order unsteady viscoelastic fluid flow over a rotating cone were studied by Saleem et al. [7]. Nadeem and Abbas [8] analyzed the flow behavior of a modified nanofluid with an exponentially stretching sheet. Hosseinzadeh et al. [9]

highlighted the impact of hybrid nanofluid flow under entropy generation. Recently, a few researchers have discovered the flow of a nanofluid with different assumptions and different geometries, as seen in the literature [10,11].

Micropolar fluids a microstructure and a non-symmetric stress tensor. By defining the nonlinear relationships of shear rate and shear stress, non-viscous liquid can be studied. The model for micropolar fluids is acceptable for biological fluids, exocytic lubricants, colloids, liquid crystals, and animal blood. There are various factors related to non-viscous liquids that can be studied during the studies of physical problems. Moreover, these fluids have a viscosity that is dependent on shear. Micropolar fluids were invented by Eringen [12]. Ahmadi [13] deliberated solutions to micropolar fluid flow considering the effects of microinertia over a semi-infinite surface. A micropolar fluid considering mixed convection toward a vertical sheet along uniform heat flux was obtained by Gorla [14]. The results of a based micropolar fluid at a stretching surface were obtained by Kelson and Desseaux [15]. The results of mixed convection of a base micropolar fluid were obtained by Bhargava et al. [16] in the presence of porous media. Qasim et al. [17] investigated steady micropolar fluid flow by considering a stretching surface along Newtonian heating. The mixed convection of base micropolar fluid under a stagnant region of a vertical sheet was explained by Ishak et al. [18]. Nadeem and Abbas [19] initiated work on hybrid nanofluid flow under slip effects. Nadeem et al. [20] analyzed micropolar fluid flow over a Riga surface. Several investigators (see Refs. [21,22]) highlighted the influence of micropolar fluid flow with various assumptions and flows on various geometries.

The slip wall condition is a case where the viscous impacts at the wall are invisible. Boundary slip is also a proper boundary condition for symmetrical surfaces. In the slip wall condition, the normal velocity is zero, but the tangential velocity is not zero. The boundary-layer theory is very effective for non-Newtonian fluid models and has received great attention in the last few years. Such flows are important in lessening the drag friction forces and enlarging the rate of transfer heat. The study of slip effects play a vital role in micropumps, micronozzles, microvalves, and hard disk drives. The no-slip condition is considered when the relative velocity between the fluid and boundary is zero. Saffman [23] studied the experiments on mass efflux and verified the presence of a non-zero tangential velocity on the surface of a permeable boundary. Chellam et al. [24] reported the impact of mass transfer as well as fluid flow in the occurrence of uniformly porous slip boundaries. Slip effects under a base micropolar fluid in vertical porous sheets were discussed by Chaudhary and Preethi [25]. Sharma [26] discussed the flow of fluctuating mass and thermal diffusion with slip conditions at a vertical plate. The MHD flow of a nanofluid with slip conditions was explored for a permeable sheet by Ibrahim and Shankar [27]. The slip effects on a porous channel with micropolar fluid in a stretching/shrinking porous medium were investigated by Xinhui et al. [28]. Several investigators (see Refs. [29,30]) have been highlighted the effects of a stretching surface.

We discussed the unsteady flow of a micropolar fluid over a curved surface. Mathematical developed under the flow assumptions, the partial differential equations are transformed into ordinary differential equations. A nonlinear system of equations was created by implementing the bvp4c numerical procedure. The effect of the physical parameters is highlighted using graphs and tables. Our current work will be helpful in the engineering and industrial fields. No one has discussed this model before. These results are utilized which helped in the fields of engineering and industry.

2. Materials and Methods

We discussed base micropolar fluids with the Buongiorno model at a permeable curved surface. In the flow direction, the arc length is s, and the normal to tangent vector is r which is shown in Figure 1a,b. Figure 1a,b shows the geometry of the stretching. The surface is stretched, where v_w is in the S-direction and c is constant, while v_w occurs because of the porous surface, which characterizes two cases: $v_w < 0$ and $v_w > 0$, which are related to injection and suction, respectively.

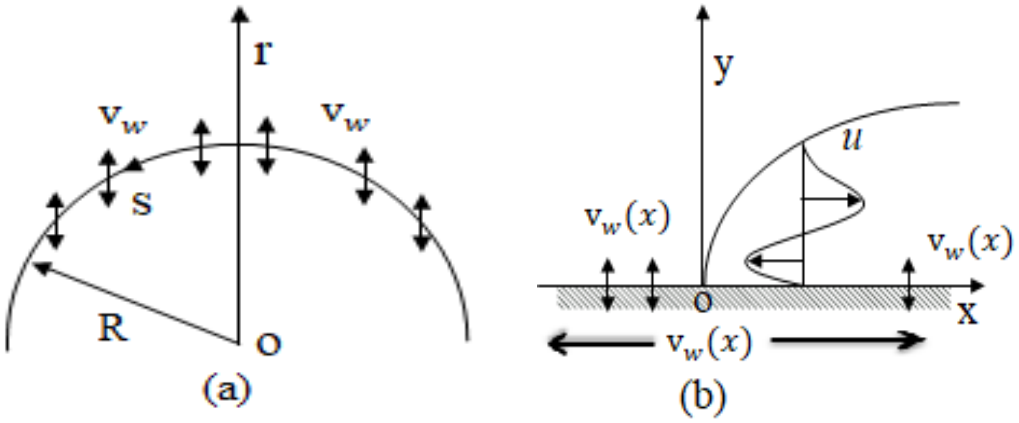

Figure 1. (**a**,**b**): Flow configuration of a curved channel.

- Unsteady flow;
- Stretching curved surface;
- Micropolar fluid flow;
- Non-linear radiation;
- Thermal slip and velocity slip.

With the boundary layer approximations as well as the above assumptions, the governing equations for the flow problem and mathematical model were developed as follows (see Refs. [31,32]):

$$\frac{1}{R+r}\frac{\partial}{\partial r}(v(r+R)) + \frac{R}{R+r}\frac{\partial u}{\partial s} = 0, \tag{1}$$

$$\frac{u^2}{R+r} = \frac{1}{\rho_f}\frac{\partial p}{\partial r}, \tag{2}$$

$$\left(\frac{\partial u}{\partial t} + v\frac{\partial u}{\partial r} + \frac{Ru}{R+r}\frac{\partial u}{\partial s} + \frac{vu}{R+r}\right) + \frac{1}{\rho_f}\frac{1}{R+r}\frac{\partial p}{\partial r} = (1+K_1)\left(\frac{\partial^2 u}{\partial^2 r} + \frac{1}{R+r}\frac{\partial u}{\partial r} - \frac{u}{(R+r)^2}\right) - \frac{K_1}{2}\frac{\partial N}{\partial r}, \tag{3}$$

$$\left(\frac{\partial N}{\partial t} + v\frac{\partial N}{\partial r} + \frac{RN}{R+r}\frac{\partial N}{\partial s}\right) = (1+K_1/2)\left(\frac{\partial^2 N}{\partial^2 r} + \frac{1}{R+r}\frac{\partial N}{\partial r}\right) - \frac{K_1}{2}\left(\frac{\partial N}{\partial r} + 2N + \frac{u}{R+r}\right), \tag{4}$$

$$\left(\frac{\partial T}{\partial t} + v\frac{\partial T}{\partial r} + \frac{Ru}{R+r}\frac{\partial T}{\partial s}\right) + \frac{\partial q_r}{\partial r} = \alpha_f\left(\frac{\partial^2 T}{\partial^2 r} + \frac{1}{R+r}\frac{\partial T}{\partial r}\right) + \left(\frac{\rho c_p}{\rho c_f}\right)\left(D_B\left(\frac{\partial C}{\partial r}\right)\left(\frac{\partial T}{\partial r}\right) + \left(\frac{D_T}{T_\infty}\right)\left(\frac{\partial T}{\partial r}\right)^2\right), \tag{5}$$

$$\left(\frac{\partial C}{\partial t} + v\frac{\partial C}{\partial r} + \frac{Ru}{R+r}\frac{\partial C}{\partial s}\right) - \left(\frac{D_T}{T_\infty}\right)\left(\frac{\partial^2 T}{\partial^2 r} + \frac{1}{R+r}\frac{\partial T}{\partial r}\right) = D_B\left(\frac{\partial^2 C}{\partial^2 r} + \frac{1}{R+r}\frac{\partial C}{\partial r}\right). \tag{6}$$

The respective boundary conditions are:

$$\begin{gathered} u = U_w + \lambda_2\left(\frac{\partial u}{\partial r} - \frac{u}{R+r}\right),\ v = V_w,\ T = T_w + \lambda_1\left(\frac{\partial T}{\partial r}\right),\ D_B\left(\frac{\partial C}{\partial r}\right) + \left(\frac{D_T}{T_\infty}\right)\left(\frac{\partial T}{\partial r}\right) = 0,\ N = -n\frac{\partial U}{\partial r},\ at\ r \to 0, \\ u \to u_\infty,\ \frac{\partial u}{\partial r} \to 0,\ N \to 0,\ T \to T_\infty,\ C \to C_\infty,\ at\ r \to \infty. \end{gathered} \tag{7}$$

The similarity variables are presented as (see Refs. [33–35]):

$$\begin{gathered} T = T_\infty + (T_w - T_\infty)\theta(\zeta),\ \zeta = \sqrt{\frac{a}{\nu_f(1-\alpha t)}}r,\ u = \frac{as}{1-\alpha t}F'(\zeta), \\ v = -\frac{R}{r+R}\sqrt{\frac{a\nu_f}{(1-\alpha t)}}F(\zeta),\ N = \frac{as}{1-\alpha t}\sqrt{\frac{a}{\nu_f(1-\alpha t)}}G(\zeta), \\ C = C_\infty + (C_w - C_\infty)\phi(\zeta),\ P = \frac{\rho a^2 s^2 p(\zeta)}{(1-\alpha t)^2}. \end{gathered} \tag{8}$$

Equation (8), for dimensionless terms, was utilized in Equations (1)–(7), which then become dimensionless, as follows:

$$P' = \frac{F'^2}{\zeta + K_0} \tag{9}$$

$$\begin{aligned}\tfrac{2K}{\zeta+K_0}P = (1+K_1)\left[F''' + \tfrac{F''}{\zeta+K_0} - \tfrac{F'}{(\zeta+K_0)^2}\right] - \tfrac{K_0}{\zeta+K_0}F'^2 + \tfrac{K_0}{\zeta+K_0}F'F'' + \tfrac{K_0}{(\zeta+K_0)^2}FF' - KG' \\ - \beta_0\left(\tfrac{\zeta}{2}F'' + F'\right),\end{aligned} \tag{10}$$

$$\left(1+\frac{K_1}{2}\right)\left[G'' + \frac{G'}{\zeta+k}\right] - \frac{K_0}{(\zeta+K_0)}F'G + \frac{K_0}{(\zeta+K_0)}FG' - K_1\left(2\mathrm{G} + F'' + \frac{1}{\zeta+K_0}F'\right) + \frac{\beta_0}{2}(\zeta G' + G), \tag{11}$$

$$\frac{1}{Pr}\left(\theta'' + \frac{1}{\zeta+K_0}\theta'\right) + \frac{K_0}{\zeta+K_0}F\theta' - \frac{K_0}{\zeta+K_0}\theta + \left(N_B\theta'\phi' + N_T\theta'\theta'\right) - \frac{\beta_0}{2}(\zeta\theta') = 0, \tag{12}$$

$$\left(\phi'' + \frac{1}{\zeta+K_0}\phi'\right) + \frac{K_0}{\zeta+K_0}F\phi' - \frac{K_0}{\zeta+K_0}\phi + \frac{N_B}{N_T}\left(\theta'' + \frac{1}{\zeta+K_0}\theta'\right) - \frac{\beta_0}{2}(\zeta\phi') = 0, \tag{13}$$

The pressure profile can be computed as

$$\begin{aligned}P(\zeta) = \tfrac{\zeta+K_0}{2K_0}\Bigg((1+K_1)\left[F''' + \tfrac{F''}{\zeta+K_0} - \tfrac{F'}{(\zeta+K_0)^2}\right] - \tfrac{K_0}{\zeta+K_0}F'^2 + \tfrac{K_0}{\zeta+K_0}F'F'' + \tfrac{K_0}{(\zeta+K_0)^2}FF' - KG' \\ - \beta_0\left(\tfrac{\zeta}{2}F'' + F'\right)\Bigg).\end{aligned}$$

Dismissing the pressure term, we obtain

$$\begin{aligned}(1+K_1)\left(F'''' + \tfrac{2}{\zeta+K_0}F''' - \tfrac{1}{(\zeta+K_0)^2}F'' + \tfrac{1}{(\zeta+K_0)^3}F'\right) - \tfrac{K_0}{\zeta+K_0}(F''F' - FF''') - \tfrac{K_0}{(\zeta+K_0)^2}\left(F'^2 - FF''\right) \\ - \tfrac{K_0}{(\zeta+K_0)^3}FF' - K\left(G'' + \tfrac{G'}{K_0+\zeta}\right) - \tfrac{\beta_0}{\zeta+K_0}\left(F' + \tfrac{\zeta}{2}F''\right) - \tfrac{\beta_0}{2}(3F'' + \zeta F''') = 0,\end{aligned} \tag{14}$$

$$\left(1+\frac{K_1}{2}\right)\left[G'' + \frac{G'}{\zeta+K_0}\right] - \frac{K_0}{(\zeta+K_0)}F'G + \frac{K_0}{(\zeta+K_0)}FG' - K_1\left(2\mathrm{G} + F'' + \frac{1}{\zeta+K_0}F'\right) + \frac{\beta_0}{2}(\zeta G' + G), \tag{15}$$

$$\frac{1}{Pr}\left(\theta'' + \frac{1}{\zeta+K_0}\theta'\right) + \frac{K_0}{\zeta+K_0}F\theta' - \frac{K_0}{\zeta+K_0}\theta + \left(N_B\theta'\phi' + N_T\theta'\theta'\right) - \frac{\beta_0}{2}(\zeta\theta') = 0, \tag{16}$$

$$\left(\phi'' + \frac{1}{\zeta+K_0}\phi'\right) + \frac{K_0}{\zeta+K_0}F\phi' - \frac{K_0}{\zeta+K_0}\phi + \frac{N_B}{N_T}\left(\theta'' + \frac{1}{\zeta+K_0}\theta'\right) - \frac{\beta_0}{2}(\zeta\phi') = 0, \tag{17}$$

with boundary conditions of

$$\begin{aligned}F(0) = \omega, \quad F'(0) = \lambda + \Pi\left(F''(0) - \tfrac{F'(0)}{K_0}\right), \quad F'(\infty) = 1, \\ F''(\infty) = 0, \quad G(0) = -nF''(0), \quad G(\infty) = 0, \quad N_B\phi'(0) + N_T\theta'(0) = 0, \\ \delta\theta'(0) + 1 = \theta(0), \quad \theta(\infty) = 0, \quad \phi(\infty) = 0.\end{aligned} \tag{18}$$

The physical interest is defined as

$$C_f = \frac{\tau_{rs}}{\rho_f u_w^2}, \quad N_s = \frac{sq_w}{k_f(T_w - T_\infty)}, \quad Sh_s = \frac{sh_m}{D_B(C_w - C_\infty)}, \quad C_m = \frac{\tau_m}{\rho_{hnf}u_w^2}, \tag{19}$$

where the quantities (τ_{rs} and q_w) are calculated as:

$$\tau_{rs} = (1+K)\left(\frac{\partial u}{\partial r} - \frac{u}{R+r}\right)_{r=0}, \quad \tau_m = (1+K/2)\left(\frac{\partial N}{\partial r} + \frac{N}{R+r}\right)_{r=0}, \\ q_w = -\left(\frac{\partial T}{\partial r}\right)_{r=0}, \; h_m = -\left(\frac{\partial C}{\partial r}\right)_{r=0}. \tag{20}$$

Using Equation (19) in Equation (20), then we obtain

$$Re_s^{-1/2} C_f = (1+K)\left(F''(0) - \frac{F'(0)}{K_0}\right), \tag{21}$$

$$Re_s C_m = \left(1 + \frac{K}{2}\right)\left(G'(0) - \frac{nF''(0)}{K_0}\right), \tag{22}$$

$$Re_s^{-1/2} N_{u_s} = -\theta'(0), \tag{23}$$

$$Re_s^{-1/2} Sh_s = -\phi'(0) \tag{24}$$

where Re_s is the local Reynold number.

3. Numerical Procedure

Equations (14)–(18) were numerically elucidated using the Matlab program, and we employed the bvp4c function to solve the above system. The tolerance level is 10^{-5}. The following procedure was available:

$$f(\zeta) = S(1);\; f'(\zeta) = S(2);\; f''(\zeta) = S(3);\; f'''(\zeta) = S(4);\; SS1 = f''''(\zeta); \\ G(\zeta) = S(5);\; G'(\zeta) = S(6);\; G''(\zeta) = SS2;\; \theta(\zeta) = S(7);\; \theta'(\zeta) = S(8);\; \theta''(\zeta) = SS3;\; \phi(\zeta) = S(9); \\ \phi'(\zeta) = S(10);\; \phi''(\zeta) = SS4; \tag{25}$$

$$SS1 = -\left(\frac{2}{x+K_0}S(4) - \frac{1}{(x+K_0)^2}S(3) + \frac{1}{(x+K_0)^3}S(2)\right) - \left(\frac{1}{(1+K_1)}\right)\left(-\frac{K_0}{x+K_0}S(3)S(2) - S(4)S(1)\right) \\ - \frac{K_0}{(x+K_0)^2}(S(2)S(2) - S(1)S(3)) - \frac{K_0}{(x+K_0)^3}S(1)S(2) - K_1\left(SS2 + \frac{S(6)}{K_0+x}\right) \\ - \frac{\beta_0}{x+K_0}\left(S(2) + \frac{x}{2}S(3)\right) - \frac{\beta_0}{2}(3S(3) + xS(4)); \tag{26}$$

$$SS2 = \frac{S(6)}{x+K_0} - \left(1 + \frac{K_1}{2}\right)^{-1}\left(-\frac{K_0}{(x+K_0)}S(2)S(5) + \frac{K_0}{(x+K_0)}S(1)S(6) - K_1\left(2S(5) + S(3) + \frac{1}{x+K_0}S(2)\right)\right. \\ \left. + \frac{\beta_0}{2}(xS(6) + S(5))\right); \tag{27}$$

$$SS3 = -\frac{S(8)}{x+K_0} - \left(\frac{1}{Pr}\right)^{-1}\left(\frac{K_0}{x+K_0}S(1)S(8) - \frac{K_0}{x+K_0}S(8) + (N_B S(7)S(10) + N_T S(8)S(8)) - \frac{\beta_0}{2}(xS(8))\right); \tag{28}$$

$$SS4 = -\left(\frac{1}{x+K_0}S(10) + \frac{K_0}{x+K_0}S(1)S(10) - \frac{K_0}{x+K_0}S(9) + \frac{N_B}{N_T}\left(SS3 + \frac{1}{x+K_0}S(8)\right) - \frac{\beta_0}{2}(xS(10))\right); \tag{29}$$

The relevant boundary conditions were

$$S0(1) - \omega;\; S0(2) - \lambda - \Pi\left(S0(3) - \frac{S0(2)}{K_0}\right);\; Sinf(2) - 1; Sinf(3);\; S0(5) + nS0(3); \\ Sinf(5);\; N_B S0(10) + N_T S0(8);\; \delta S0(8) + 1 - S0(7);\; Sinf(7);\; Sinf(9); \tag{30}$$

4. Results and Discussion

The present problem was solved numerically by using the bvp4c/shooting procedure. The effect of distinct parameters is graphically portrayed along the temperature and concentration profiles. Figures 2–5 depict the variation in temperature profiles along the distinct values of flow parameters. Figure 2 shows that by enlarging the value of the unsteadiness parameter β_0, the temperature profile declines for in the cases of both suction and injection. A physical increase in β_0 causes an increase in the thickness of the thermal layer. In Figure 3, the variation in the temperature plot is displayed against the thermophoresis parameter. Figure 3 shows the impacts of N_T on the temperature profile. The temperature profile

reduced due to increasing values of N_T. Physically, N_T is directly proportional to the heat thermal coefficient which arises with fluid; hence, the heat transfer rate at the surface diminishes. In Figure 4, the variation in the temperature plot is displayed against the thermal slip parameter. Figure 4 reveals that the value of δ increases when the temperature plot is reduced. Physically, δ is directly proportional to the heat thermal coefficient which arises with fluid; hence, the heat transfer rate at the surface diminishes. In Figure 5, it is shown that $\theta(\zeta)$ decreases with greater values of K_0 in the cases of both suction and injection. Figures 6 and 7 illustrate the variation in the concentration field for altered values of physical parameters. Figure 6 shows the diversity in the concentration profile for different values of the unsteadiness parameter. It is clarified that the concentration field decreases for the parameter of β_0 in the cases of both suction and injection. Figure 7 shows that the concentration field is reduced due to enhancement in the values of N_B.

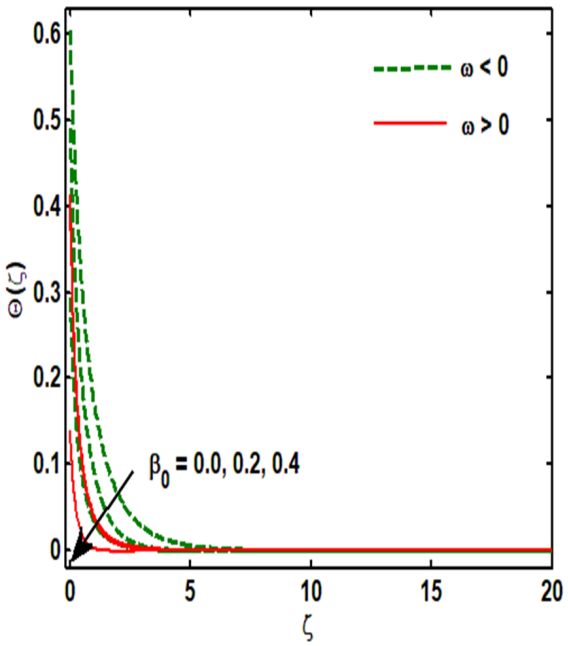

Figure 2. Influence of β_0 on temperature.

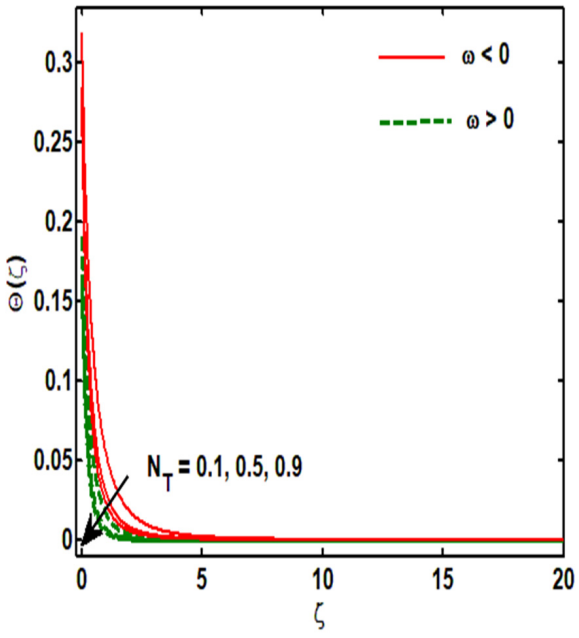

Figure 3. Influence of N_T on temperature.

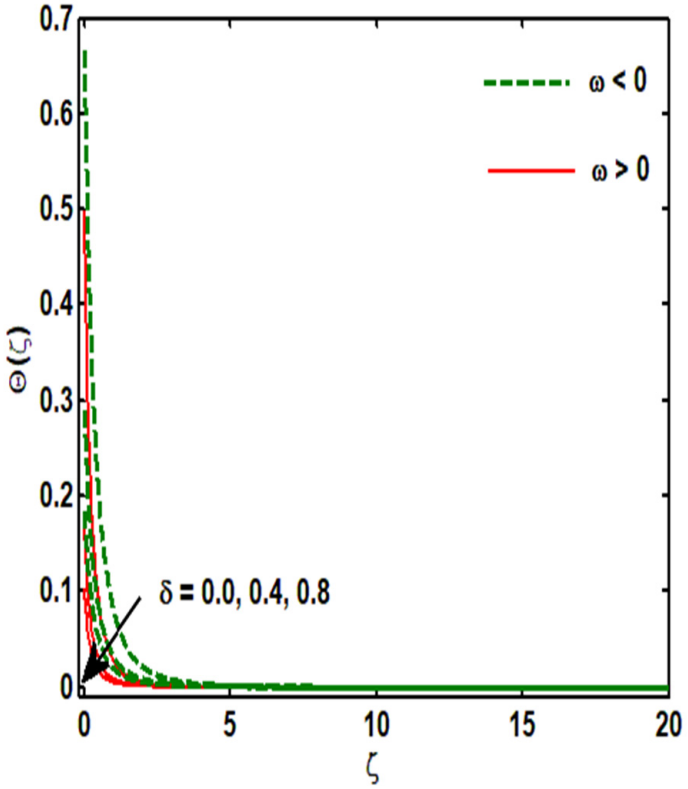

Figure 4. Influence of δ on temperature.

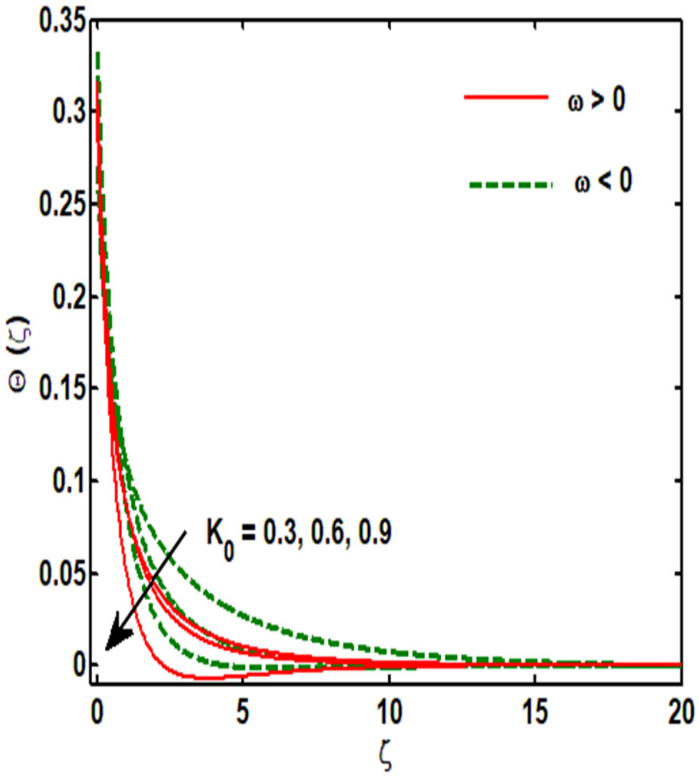

Figure 5. Influence of K_0 on temperature.

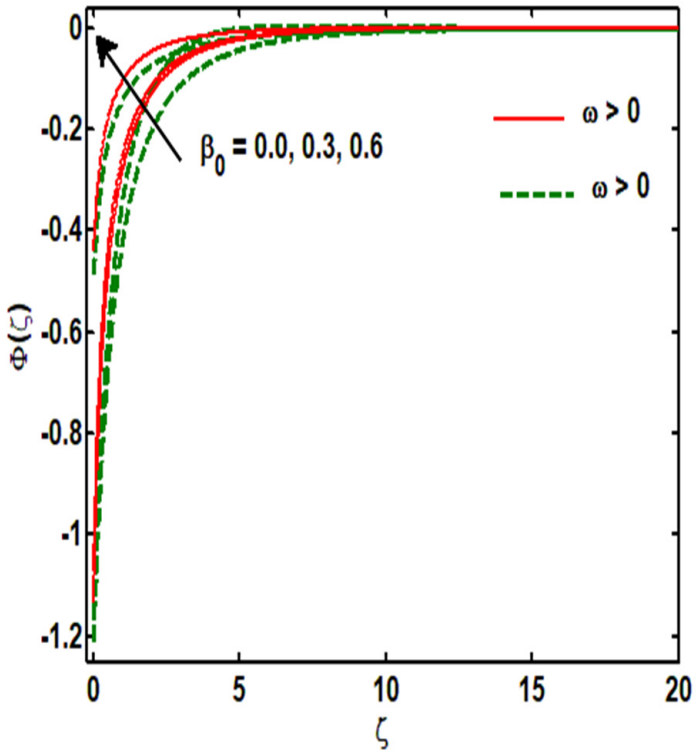

Figure 6. Influence of β_0 on temperature.

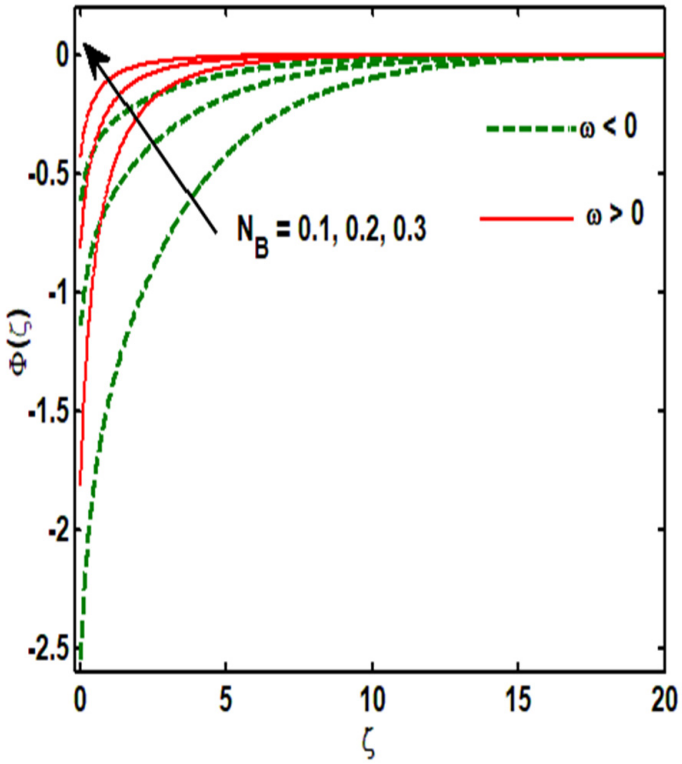

Figure 7. Influence of N_B on temperature.

Tables 1 and 2 present the influence of several physical parameters on the $Re_s^{1/2}C_f$, $Re_s^{1/2}N_{u_s}$, and $Re_s^{1/2}C_m$ for micropolar nanofluid. We also acknowledge the influence of strong and weak concentrations. The effects of δ on $Re_s^{1/2}N_{u_s}$ are shown. It is noted that δ increases as the value of $Re_s^{1/2}N_{u_s}$ decreases, because the thermal slip reduces the heat transfer rate on the curved surface. The value of $Re_s^{1/2}N_{u_s}$ declines in the case of a weak concentration correlated to a strong concentration. Thermal slip does not influence $Re_s^{1/2}C_f$ or $Re_s^{1/2}C_m$. In terms of the impacts of Π on $Re_s^{1/2}C_f$, $Re_s^{1/2}N_{u_s}$, and $Re_s^{1/2}C_m$, it is observed that the value of Π increases as the values of $Re_s^{1/2}C_f$, $Re_s^{1/2}N_{u_s}$, and $Re_s^{1/2}C_m$ increase, because the slip velocity increases, which increased in heat transfer, $Re_s^{1/2}C_m$, or skin frictions because the motion of the fluid flow increases. The $Re_s^{1/2}C_f$, $Re_s^{1/2}N_{u_s}$, and $Re_s^{1/2}C_m$ values decline when a weak concentration is correlated to a strong concentration. In terms of the influence of λ on the $Re_s^{1/2}C_f$, $Re_s^{1/2}N_{u_s}$, and $Re_s^{1/2}C_m$ values, it is observed that the value of λ increases as the $Re_s^{1/2}C_f$, $Re_s^{1/2}N_{u_s}$, and $Re_s^{1/2}C_m$ values increase which increase in heat transfer, $Re_s^{1/2}C_m$, and skin frictions due to the increase in the motion of the fluid flow. In terms of the influence of ω on the $Re_s^{1/2}C_f$, $Re_s^{1/2}N_{u_s}$, and $Re_s^{1/2}C_m$, it is seen that the values of $Re_s^{1/2}C_f$ and $Re_s^{1/2}C_m$ decrease with an increase in ω due to the suction flow, which prevents any decreases in the skin friction and $Re_s^{1/2}C_m$. Meanwhile, the $Re_s^{1/2}N_{u_s}$ value increases as the ω heat transfer rate increases. The $Re_s^{1/2}C_f$, $Re_s^{1/2}N_{u_s}$, and $Re_s^{1/2}C_m$ values decrease in the case of $n = 0.5$ compared to when $n = 0$. In terms of the impact of K_0 on the $Re_s^{1/2}C_f$, $Re_s^{1/2}N_{u_s}$, and $Re_s^{1/2}C_m$, it is seen that the $Re_s^{1/2}C_f$ and $Re_s^{1/2}C_m$ values decrease with an increase in K_0 due to the increased values of curvature, which force a reduction in the skin friction and $Re_s^{1/2}C_m$ values. Meanwhile, the $Re_s^{1/2}N_{u_s}$ value increases with larger values of K_0 because the increases in the values of the curvature parameter prevent the heat transfer rate at the surface from increasing. The $Re_s^{1/2}C_f$, $Re_s^{1/2}N_{u_s}$, and $Re_s^{1/2}C_m$ values decrease in the case of a weak concentration as compared to that of a strong concentration. In terms of the effects of K_1 on $Re_s^{1/2}C_f$, $Re_s^{1/2}N_{u_s}$, and $Re_s^{1/2}C_m$, it is seen that the $Re_s^{1/2}C_f$ and $Re_s^{1/2}C_m$ values increase with an increase in K_1 because the values of the micropolar parameter are increased, which prevent any decreases in skin friction and $Re_s^{1/2}C_m$. Meanwhile, the $Re_s^{1/2}N_{u_s}$ value decreases as the value of K_1 increases, because decreasing the values of the micropolar parameter forces reductions to the heat transfer rate at the surface to occur. In terms of the influence of T_0 on $Re_s^{1/2}C_f$, $Re_s^{1/2}N_{u_s}$, and $Re_s^{1/2}C_m$, it is seen that the $Re_s^{1/2}C_f$ and $Re_s^{1/2}C_m$ values increase with an increase in T_0 because the skin friction enhances due to the heat, while $Re_s^{1/2}N_{u_s}$ declines with as the values of T_0 increase because radiation increases, which reduces the heat transfer rate at the surface. In terms of the impact of N_T on $Re_s^{1/2}N_{u_s}$, it is noted that N_T increases as $Re_s^{1/2}N_{u_s}$ increases because the small number of nanoparticles enhances the heat transfer rate of the wall. There are no effects of thermal slip on $Re_s^{1/2}C_f$ and $Re_s^{1/2}C_m$. The impact of N_B on $Re_s^{1/2}N_{u_s}$ is shown. It is noted that N_B increases with decreased $Re_s^{1/2}N_{u_s}$ due to the collision of fluid and nanoparticles, which reduce the heat transfer rate at the surface. No impacts of δ on $Re_s^{1/2}C_f$ or $Re_s^{1/2}C_m$ were found. In terms of the effects of β_0 on $Re_s^{1/2}C_f$, $Re_s^{1/2}N_{u_s}$, and $Re_s^{1/2}C_m$, it is seen that the $Re_s^{1/2}C_f$ and $Re_s^{1/2}C_m$ values increase with an increase in β_0, while $Re_s^{1/2}N_{u_s}$ decreases with larger values of β_0, because the decreasing values of unsteadiness force a decline in the heat transfer rate at the surface. Table 3 compares the present analysis with Nogrehabadi et al. [36] and Sahoo and Do [37] for $Re_s^{1/2}C_f$ with diverse values of the suction parameter.

Table 1. Computational analysis of $Re_s^{1/2}C_f$, $Re_s^{1/2}N_{u_s}$, and $Re_s^{1/2}C_m$ for physical values when $n = 0.0$.

β_0	N_B	N_T	T_0	K_1	K_0	ω	λ	Π	δ	$Re_s^{1/2}N_{u_s}$	$Re_s^{1/2}C_f$	$Re_s^{1/2}C_m$
0.10	0.5	0.5	0.5	0.5	0.5	0.4	0.4	0.4	0.4	1.2700	0.3774	−0.6640
0.30										1.0252	1.6475	−1.5880
0.50										0.3034	1.8409	−2.3542
0.70										0.0525	2.2916	−3.4971
0.50	0.10									1.3240	1.5409	−3.3542
	0.30									1.3170	1.5409	−3.3542
	0.50									1.3034	1.5409	−3.3542
	0.70									1.2840	1.5409	−3.3542
	0.50	0.10								1.2245	1.5409	−3.3542
		0.30								1.2862	1.5409	−3.3542
		0.50								1.3034	1.5409	−3.3542
		0.70								1.3137	1.5409	−3.3542
		0.50	0.10							1.4242	1.3640	−2.8175
			0.30							1.3583	1.4737	−3.0859
			0.50							1.3034	1.5409	−3.3542
			0.70							1.2569	1.5655	−3.6225
			0.50	0.10						1.2831	−0.7659	−0.5922
				0.30						1.2956	1.6675	−1.1999
				0.50						1.3296	1.8126	−2.2200
				0.70						1.8271	2.2740	2.5751
				0.50	0.10					1.3156	−0.8746	−0.3638
					0.30					1.2361	−1.2702	−1.1912
					0.50					1.1296	−1.5126	−1.2200
					0.70					1.0426	−2.4959	−1.6223
					0.50	0.00				1.2849	2.1518	−4.0259
						0.20				1.3074	1.8256	−3.6167
						0.40				1.3296	1.5126	−3.2200
						0.60				1.3514	1.2097	−2.8323
						0.40	0.00			1.0927	−1.4449	−2.6394
							0.20			1.1381	−1.6614	−3.0333
							0.40			1.3296	−1.8126	−3.2200
							0.60			1.3370	−2.0450	−3.4929
							0.40	0.00		1.0863	0.9174	−2.0755
								0.20		1.2045	−1.3762	−2.2529
								0.40		1.3296	−1.5126	−3.2200
								0.60		1.4658	−2.0693	−3.4202
								0.40	0.00	2.7467	1.5126	−3.2200
									0.20	1.7981	1.5126	−3.2200
									0.40	1.3296	1.5126	−3.2200
									0.60	1.0529	1.5126	−3.2200

Table 2. Computational analysis of $Re_s^{1/2}C_f$, $Re_s^{1/2}N_{u_s}$, and $Re_s^{1/2}C_m$ for physical values when $n = 0.5$.

β_0	N_B	N_T	T_0	K_1	K_0	ω	λ	Π	δ	$Re_s^{1/2}N_{u_s}$	$Re_s^{1/2}C_f$	$Re_s^{1/2}C_m$
0.10	0.5	0.5	0.5	0.5	0.5	0.4	0.4	0.4	0.4	1.2387	−0.4436	−0.4829
0.30										1.3774	−0.5491	−0.5038
0.50										1.4413	−1.0546	−1.4398
0.70										1.5472	−1.1999	−1.7156
0.50	0.10									1.1634	−1.0546	−1.4398
	0.30									1.0559	−1.0546	−1.4398
	0.50									1.0413	−1.0546	−1.4398
	0.70									1.0206	−1.0546	−1.4398
	0.50	0.10								0.9572	−1.0546	−1.4398
		0.30								1.0226	−1.0546	−1.4398
		0.50								1.0413	−1.0546	−1.4398
		0.70								1.0526	−1.0546	−1.4398
		0.50	0.10							1.1131	−0.9813	−1.2598
			0.30							1.0630	−1.0395	−1.3798
			0.50							1.0215	−1.0606	−1.4998
			0.70							0.9862	−1.0447	−1.6198
			0.50	0.10						0.9124	−2.2180	−1.5941
				0.30						1.0343	−1.3561	−1.5290
				0.50						1.0413	−1.0546	−1.4398
				0.70						0.5037	−22.9779	10.7449
				0.50	0.10					1.5078	−1.9102	−1.9608
					0.30					0.6701	−1.3918	−2.1640
					0.50					0.3413	−1.0546	−2.4398
					0.70					0.1856	−1.0211	−3.2148
					0.50	0.00				0.9768	−1.0076	−1.2888
						0.20				1.0094	−1.0319	−1.3616
						0.40				1.0413	−1.0546	−1.4398
						0.60				1.0727	−1.0764	−1.5233
						0.40	0.00			1.0273	−1.0219	−1.1099
							0.20			1.0362	−1.0530	−1.3134
							0.40			1.0413	−1.0546	−1.4398
							0.60			1.2837	−1.0807	−1.5794
							0.40	0.00		0.5517	−1.0230	−0.7457
								0.20		0.6602	−1.0463	−0.8614
								0.40		1.0413	−1.0546	−1.4398
								0.60		1.2326	−1.0736	−1.6826
								0.40	0.00	2.1024	−1.0546	−1.4398
									0.20	1.3965	−1.0546	−1.4398
									0.40	1.0413	−1.0546	−1.4398
									0.60	0.8296	−1.0546	−1.4398

Table 3. The present results compared with Nogrehabadi et al. [36] and Sahoo and Do [37] for $Re_s^{1/2}C_f$ when rest of physical parameters are zero and $K_0 \to 10,000$.

ω	Sahoo and Do [33]	Nogrehabadi et al. [34]	Present Results
0.00	1.00112	1.00021	1.00001
0.10	0.87143	0.87204	0.871721
0.20	0.77491	0.77633	0.776014
0.30	0.69974	0.70152	0.700910
0.50	0.58912	0.59110	0.591021
1.00	0.42841	0.43011	0.430211

5. Final Remarks

We analyzed micropolar fluid flow over a stretched curved surface. The results of the dimensionless system and physical parameters that appeared under the flow assumptions were elaborated upon through graphs and tables. The main achievements of the current analysis are highlighted below:

- In terms of the values of $Re_s^{1/2}C_f$, $Re_s^{1/2}N_{u_s}$, and $Re_s^{1/2}C_m$, a weak concentration $(n = 0.5)$ enables greater values in comparison to a strong concentration $(n = 0.0)$.
- The temperature profile achieves greater values near the surface in the case of $\omega > 0$ as compared to $\omega < 0$.
- Surprisingly, the concentration profile achieves greater values near the surface in the case of $\omega > 0$ as compared to $\omega < 0$ due to increments in the β_0 and N_B.
- The unsteadiness parameter increases, which resists increases in the Nusselt number in a strong concentration $(n = 0.0)$ but declines in a weak concentration $(n = 0.5)$.
- The thermophoresis parameter increases as the Nusselt number increases because the small number of nanoparticles enhances the heat transfer rate.
- The higher value of the unsteadiness parameter β_0, the lower the temperature profile for the cases of both suction and injection.

Author Contributions: N.A. wrote the manuscript under the supervision of W.S. All authors have read and agreed to the published version of the manuscript.

Funding: The authors would like to acknowledge the support of Prince Sultan University for paying the Article Publication Fee of this publication.

Institutional Review Board Statement: Not applicable.

Informed Consent Statement: Not applicable.

Data Availability Statement: Not applicable.

Acknowledgments: We are thankful to the anonymous referees for their valuable comments, which helped us improve the paper's quality. The authors wish to express their gratitude to Prince Sultan University for facilitating the publication of this article through the research lab Theoretical and Applied Sciences Lab.

Conflicts of Interest: The authors declare no conflict of interest.

Nomenclature

ϵ (1)	Non-dimensional parameter
Re_s (1)	Reynolds number
λ (1)	Stretching parameter
N (m/s)	Angular velocity components
u, v (m)	Velocity components

K_0 (1)	Curvature parameter
u (m/s)	Velocity vector r-direction
Sh_s (1)	Sherwood number
N_T (1)	Thermophoresis parameter
n (1)	Microgyration
ω (1)	Stretching parameter
α (m^2/s)	Thermal diffusivity
T (K)	Temperature
T_w (K)	Wall temperature
λ (1)	Stretching parameter
K_1 (1)	Micropolar parameter
k (Ns/m^2)	Vertex viscosity
$(c_p)_f$ (J/kg K)	Heat capacity of fluid
s (m)	Arc length
N_B (1)	Brownian motion parameter
τ_{rs} (pa)	Wall shear stress
T_w (K)	Wall temperature
Pr (1)	Prandtl number
R (m)	Radius of curvature
ρ (kg/m^3)	Fluid density
T_∞ (K)	Ambient temperature
μ (Ns/m^2)	Dynamic viscosity
T_∞ (K)	Ambient temperature
Π (1)	Velocity slip

References

1. Choi, S.U.; Eastman, J.A. *Enhancing Thermal Conductivity of Fluids with Nanoparticles (No. ANL/MSD/CP-84938; CONF-951135-29)*; Argonne National Lab.: Lemont, IL, USA, 1995.
2. Masuda, H.; Ebata, A.; Teramae, K. Alteration of thermal conductivity and viscosity of liquid by dispersing ultra-fine particles. Dispersion of Al_2O_3, SiO_2 and TiO_2 ultra-fine particles. *Netsu Bussei* **1993**, *7*, 227–233. [CrossRef]
3. Yu, W.; Mittra, R. A conformal finite difference time domain technique for modeling curved dielectric surfaces. *IEEE Microw. Wirel. Compon. Lett.* **2001**, *11*, 25–27. [CrossRef]
4. Nadeem, S.; Lee, C. Boundary layer flow of nanofluid over an exponentially stretching surface. *Nanoscale Res. Lett.* **2012**, *7*, 94. [CrossRef] [PubMed]
5. Nadeem, S.; Maraj, E. The mathematical analysis for peristaltic flow of hyperbolic tangent fluid in a curved channel. *Commun. Theor. Phys.* **2013**, *59*, 729–736. [CrossRef]
6. Malvandi, A.; Hedayati, F.; Nobari, M.R.H. An HAM analysis of stagnation-point flow of a nanofluid over a porous stretching sheet with heat generation. *J. Appl. Fluid Mech.* **2014**, *7*, 135–145.
7. Saleem, S.; Nadeem, S.; Awais, M. Time-dependent second-order viscoelastic fluid flow on rotating cone with heat generation and chemical reaction. *J. Aerosp. Eng.* **2016**, *29*, 4. [CrossRef]
8. Nadeem, S.; Abbas, N. Effects of MHD on modified nanofluid model with variable viscosity in a porous medium. In *Nanofluid Flow in Porous Media*; IntechOpen: London, UK, 2019; pp. 109–117. [CrossRef]
9. Hosseinzadeh, K.; Mardani, M.R.; Salehi, S.; Paikar, M.; Waqas, M.; Ganji, D.D. Entropy generation of three-dimensional Bödewadt flow of water and hexanol base fluid suspended by Fe_3O_4 and MoS_2 hybrid nanoparticles. *Pramana* **2021**, *95*, 57. [CrossRef]
10. Hosseinzadeh, K.; Roghani, S.; Mogharrebi, A.R.; Asadi, A.; Ganji, D.D. Optimization of hybrid nanoparticles with mixture fluid flow in an octagonal porous medium by effect of radiation and magnetic field. *J. Therm. Anal.* **2021**, *143*, 1413–1424. [CrossRef]
11. Abbas, N.; Shatanawi, W. Heat and mass transfer of micropolar-casson nanofluid over vertical variable stretching riga sheet. *Energies* **2022**, *15*, 4945. [CrossRef]
12. Eringen, A.C. Theory of micropolar fluids. *J. Math. Mech.* **1966**, *16*, 1–18. [CrossRef]
13. Ahmadi, G. Self-similar solution of imcompressible micropolar boundary layer flow over a semi-infinite plate. *Int. J. Eng. Sci.* **1976**, *14*, 639–646. [CrossRef]
14. Gorla, R.S.R. Mixed convection in a micropolar fluid from a vertical surface with uniform heat flux. *Int. J. Eng. Sci.* **1992**, *30*, 349–358. [CrossRef]
15. Kelson, N.; Desseaux, A. Effect of surface conditions on flow of a micropolar fluid driven by a porous stretching sheet. *Int. J. Eng. Sci.* **2001**, *39*, 1881–1897. [CrossRef]
16. Bhargava, R.; Kumar, L.; Takhar, H. Finite element solution of mixed convection micropolar flow driven by a porous stretching sheet. *Int. J. Eng. Sci.* **2003**, *41*, 2161–2178. [CrossRef]

17. Qasim, M.; Khan, I.; Shafie, S. Heat transfer in a micropolar fluid over a stretching sheet with newtonian heating. *PLoS ONE* **2013**, *8*, e59393. [CrossRef] [PubMed]
18. Ishak, A.; Nazar, R.; Pop, I. Magnetohydrodynamic (MHD) flow of a micropolar fluid towards a stagnation point on a vertical surface. *Comput. Math. Appl.* **2008**, *56*, 3188–3194. [CrossRef]
19. Nadeem, S.; Abbas, N. On both MHD and slip effect in micropolar hybrid nanofluid past a circular cylinder under stagnation point region. *Can. J. Phys.* **2018**, *97*, 392–399. [CrossRef]
20. Nadeem, S.; Malik, M.Y.; Abbas, N. Heat transfer of three-dimensional micropolar fluid on a Riga plate. *Can. J. Phys.* **2019**, *98*, 32–38. [CrossRef]
21. Abbas, N.; Rehman, K.U.; Shatanawi, W.; Al-Eid, A.A. Theoretical study of non-Newtonian micropolar nanofluid flow over an ex-ponentially stretching surface with free stream velocity. *Adv. Mech. Eng.* **2022**, *14*, 16878132221107790. [CrossRef]
22. Fuzhang, W.; Anwar, M.I.; Ali, M.; El-Shafay, A.S.; Abbas, N.; Ali, R. Inspections of unsteady micropolar nanofluid model over ex-ponentially stretching curved surface with chemical reaction. *Waves Random Complex Media* **2022**, 1–22. [CrossRef]
23. Saffman, P.G. On the boundary condition at the surface of a porous medium. *Stud. Appl. Math.* **1971**, *50*, 93–101. [CrossRef]
24. Chellam, S.; Wiesner, M.R.; Dawson, C. Slip at a uniformly porous boundary: Effect on fluid flow and mass transfer. *J. Eng. Math.* **1992**, *26*, 481–492. [CrossRef]
25. Sharma, P.K.; Chaudhary, R.C. Effect of variable suction on transient free convection viscous incompressible flow past a vertical plate with periodic temperature variations in slip-flow regime. *Emir. J. Eng. Res.* **2003**, *8*, 33–38.
26. Sharma, P.K. Fluctuating thermal and mass diffusion on unsteady free convection flow past a vertical plate in slip-flow regime. *Lat. Am. Appl. Res.* **2005**, *35*, 313–319.
27. Ibrahim, W.; Shankar, B. MHD boundary layer flow and heat transfer of a nanofluid past a permeable stretching sheet with velocity, thermal and solutal slip boundary conditions. *Comput. Fluids* **2013**, *75*, 1–10. [CrossRef]
28. Xinhui, S.; Liancun, Z.; Xuehui, C.; Xinxin, Z.; Limei, C.; Min, L. The effects of slip velocity on a micropolar fluid through a porous channel with expanding or contracting walls. *Comput. Methods Biomech. Biomed. Eng.* **2014**, *17*, 423–432. [CrossRef] [PubMed]
29. Abbas, N.; Rehman, K.U.; Shatanawi, W.; Malik, M. Numerical study of heat transfer in hybrid nanofluid flow over permeable nonlinear stretching curved surface with thermal slip. *Int. Commun. Heat Mass Transf.* **2022**, *135*, 106107. [CrossRef]
30. Abbas, N.; Nadeem, S.; Khan, M.N. Numerical analysis of unsteady magnetized micropolar fluid flow over a curved surface. *J. Therm. Anal.* **2021**, *147*, 6449–6459. [CrossRef]
31. Amjad, M.; Zehra, I.; Nadeem, S.; Abbas, N. Thermal analysis of Casson micropolar nanofluid flow over a permeable curved stretching surface under the stagnation region. *J. Therm. Anal.* **2021**, *143*, 2485–2497. [CrossRef]
32. Nadeem, S.; Abbas, N.; Malik, M. Inspection of hybrid based nanofluid flow over a curved surface. *Comput. Methods Programs Biomed.* **2020**, *189*, 105193. [CrossRef]
33. Abbas, N.; Shatanawi, W.; Abodayeh, K. Computational Analysis of MHD Nonlinear Radiation Casson Hybrid Nanofluid Flow at Vertical Stretching Sheet. *Symmetry* **2022**, *14*, 1494. [CrossRef]
34. Abbas, N.; Nadeem, S.; Saleem, A. Computational analysis of water based Cu-Al_2O_3/H_2O flow over a vertical wedge. *Adv. Mech. Eng.* **2020**, *12*, 1687814020968322. [CrossRef]
35. Ahmad, S.; Khan, Z.H. Numerical solution of micropolar fluid flow with heat transfer by finite difference method. *Int. J. Mod. Phys. B* **2022**, *36*, 2250037. [CrossRef]
36. Noghrehabadi, A.; Pourrajab, R.; Ghalambaz, M. Effect of partial slip boundary condition on the flow and heat transfer of nanofluids past stretching sheet prescribed constant wall temperature. *Int. J. Therm. Sci.* **2012**, *54*, 253–261. [CrossRef]
37. Sahoo, B.; Poncet, S. Flow and heat transfer of a third grade fluid past an exponentially stretching sheet with partial slip boundary condition. *Int. J. Heat Mass Transf.* **2011**, *54*, 5010–5019. [CrossRef]